



## Investigation of variability of iron emission lines in Centaurus X-3

Sachindra Naik<sup>1\*</sup> and Biswajit Paul<sup>2†</sup>

<sup>1</sup>Physical Research Laboratory, Navrangpura, Ahmedabad 380009, Gujarat, India

<sup>2</sup>Raman Research Institute, Sadashivnagar, C. V. Raman Avenue, Bangalore 560080, India

Received 2012 July 31; accepted 2012 November 13

**Abstract.** We present the results obtained from a study of the variability of iron emission lines in the high mass X-ray binary pulsar Cen X-3 during the eclipse, eclipse-egress and out-of-eclipse phases using *XMM – Newton* observations. Three iron emission lines at 6.4 keV, 6.7 keV, and 6.97 keV are clearly detected in the spectrum of the pulsar during the entire observations, irrespective of different binary phases. The properties of these emission lines are investigated at different intensity levels. The flux level and equivalent width of the emission lines change during the eclipse, eclipse-egress and out-of-eclipse orbital phases. Based on the results obtained from the time resolved spectral analysis, it is understood that the most probable emitting region of 6.4 keV fluorescent line is very close to the neutron star whereas the other two lines are produced in a region that is far from the neutron star, probably in the highly photo-ionized wind of the companion star or in the accretion disk corona.

**Keywords :** stars: binaries: general – stars: pulsars: general – stars: neutron – X-rays: binaries – X-rays: individual: Cen X-3

### 1. Introduction

Centaurus X-3 is the first X-ray source to be discovered as an accretion powered X-ray binary pulsar (Giacconi et al. 1971). It is one of the brightest accreting X-ray pulsars. It was discovered from observations made with a rocket-based detector (Chodil et al. 1967) and later satellite observations revealed its binary and pulsar nature (Giacconi et al. 1971; Schreier et al. 1972). The optical companion was found to be an O-type supergiant star V779 Cen (Krzeminski 1974)

---

\*email: snaik@prl.res.in

†email: bpaul@rri.res.in

that has a radius of  $\sim 12 R_{\odot}$  and a mass of  $\sim 17-19 M_{\odot}$  (Hutchings et al. 1979). The distance to the binary system is estimated to be  $\sim 8$  kpc (Krzeminski 1974). It is an eclipsing High Mass X-ray Binary (HMXB) pulsar. The X-ray data show eclipses for  $\sim 20\%$  of the binary orbit (see Nagase 1989). The pulse period of the pulsar was estimated to be  $\sim 4.8$  s (Schreier et al. 1972) and an orbital period of  $\sim 2.1$  days (Nagase 1989). The high value of observed luminosity of the pulsar ( $\sim 5 \times 10^{37}$  erg s $^{-1}$ ) suggests that the predominant mode of accretion is via accretion disk, fed by a Roche-lobe overflow (Tjemkes et al. 1986). The optical light curve (Tjemkes et al. 1986) also indicates the presence of an accretion disk, fed by Roche lobe overflow. The long term RXTE-All Sky Monitor (ASM) light curve of Cen X-3 shows a succession of high and low intensity states, which appear to be random. It was found from the RXTE-ASM data that even in different energy bands, Cen X-3 had a flux  $\sim 40$  times larger during the high/outburst states as compared to the low state (Paul et al. 2005). It was also reported that the low and high states last between a few days to  $\sim 110$  days, without having any periodicity (Paul et al. 2005).

The broadband, out-of-eclipse phase-averaged spectrum of Cen X-3 has been described by an absorbed power-law, a broad iron emission line at  $\sim 6.7$  keV along with a high energy cut-off at  $\sim 14$  keV (Burderi et al. 2000). A soft excess detected in the spectrum below 1 keV is interpreted as a black-body with temperature  $kT \sim 0.1$  keV (Burderi et al. 2000) that is now known to be present in many X-ray pulsars (Paul et al. 2002; Naik & Paul 2003, 2004 and references therein). From *BeppoSAX* observations of the pulsar, a cyclotron resonance feature at  $\sim 28$  keV has also been detected and the corresponding magnetic field strength was estimated to be  $B \sim (2.4-3.0) \times 10^{12}$  G (Santangelo et al. 1998). A number of emission lines are expected in the X-ray spectrum of this source due to its high X-ray luminosity and the presence of a stellar wind from the companion star at a distance of only 40 lt-s (Kelley et al. 1983; Ebisawa et al. 1996; Wojdowsky et al. 2003; Iaria et al. 2005). In the spectrum obtained from the *ASCA* observations of the pulsar, emission lines from hydrogenic ions of Ne, Mg, Si, and S were observed along with clearly resolved 6.4 keV, 6.7 keV, and 6.97 keV iron emission lines (Ebisawa et al. 1996). The three iron emission lines are known to originate from neutral or lowly ionized iron, helium-like iron and hydrogen-like iron, respectively. A long *Suzaku* observation of Cen X-3, covering nearly one orbital period, revealed the presence of extended dips in the light curve which are rarely seen in HMXBs. These dips are seen up to as high as  $\sim 40$  keV (Naik et al. 2011). The broad band energy spectrum (in 0.5–70 keV range) obtained from the *Suzaku* observations was found to be well described by a partial covering power law model with high energy cut-off and three Gaussian functions for 6.4 keV, 6.7 keV, and 6.97 keV iron emission lines. The observed dips in the X-ray light curve were explained by the presence of additional absorption component with high column density and covering fraction. The iron line parameters during the dips and eclipse were found to be significantly different compared to those during the rest of the observations.

In the present work, we have carried out spectral analysis of Cen X-3 to investigate the emitting regions and evolution of three iron emission lines during eclipse, eclipse-egress and normal intensity out-of-eclipse phases using *XMM-Newton* observations of the pulsar. For this purpose, we describe the observations, data analysis and results in the following Section. Then in the next section, we discuss the results.

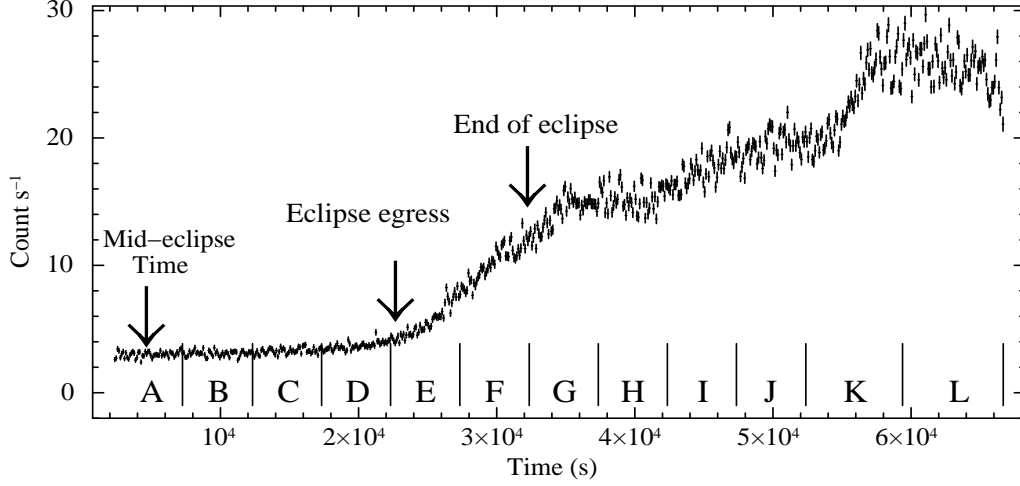


**Figure 1.** Light curve (with 100 s binning time) obtained from *XMM – Newton* observations of the high mass X-ray binary pulsar Cen X-3. Data from EPIC-PN detector is plotted here. The mid-eclipse time and the end of eclipse (including eclipse-egress) of the pulsar are marked in the figure. The entire light curve is divided into various segments (marked with letters) for the time-resolved spectroscopy as described in the following section.

## 2. Observations, analyses and results

Cen X-3 was observed with *XMM – Newton* on 2001 January 27 with its European Photon Imaging Camera (EPIC). The observations were carried out by using medium filters for all three focal plane instruments MOS-1, MOS-2 and PN for an exposure of  $\sim 68$  ks. Data from MOS-1 camera was not considered in this work as the instrument was operated in “fast uncompress mode”. Though MOS-2 was operated in “full frame mode” and PN was operated in “small window mode”, the photon pile-up during these observations was negligible for both the cameras. Though the pulsar is very bright in X-rays, the *XMM – Newton* observations were made during the eclipse and eclipse-egress during which a significant fraction of the source photons were blocked by the optical companion. At the same time, the effect of photon pile-up, if any when the pulsar was out-of-eclipse towards the end of the observations, does not have any significant effect on the study of evolution of three closely spaced iron emission lines over orbital phase of the pulsar. The raw events from PN and MOS-2 cameras were processed and filtered using the *XMM – Newton* Science Analysis System (SAS). The light curves and spectra were extracted from a circular region of  $40''$  radius, centered at the source position. The background light curves and spectra were extracted from source-free regions with a circular region of the same area as the source region. The EPIC-PN and MOS responses were generated using the SAS tasks *arfgen* and *rmfgen*. It is also to be mentioned that there was a background flare during the last 2 ks of the data (from 66 ks to 68 ks). Hence we did not use this portion in our spectral analysis.

Light curves were extracted from the event data. It is found that the PN and MOS-2 light

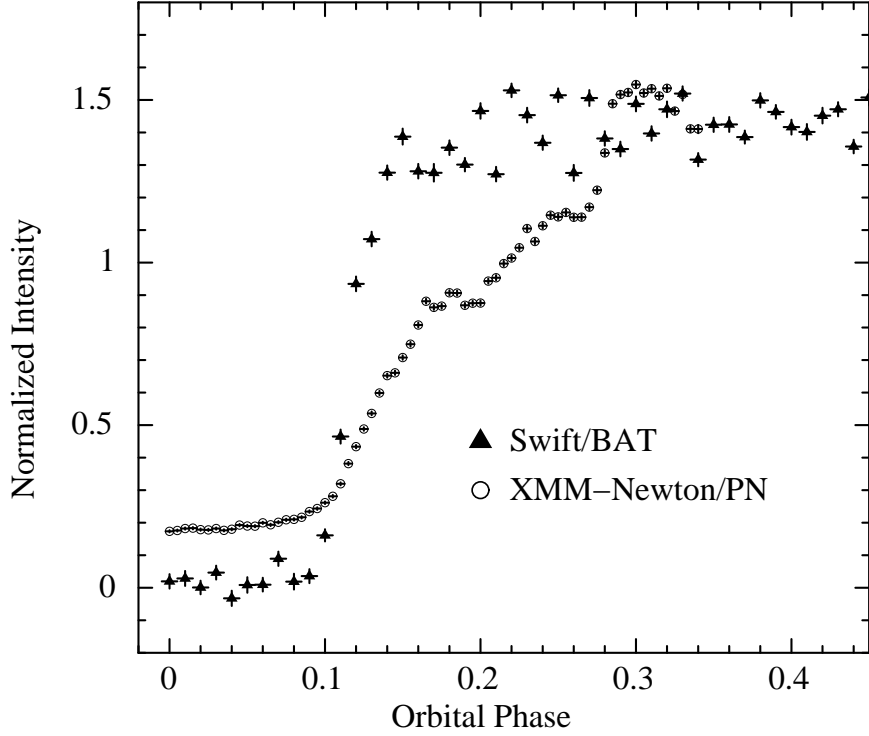


**Figure 2.** The orbital modulation in soft X-ray (*XMM – Newton*/PN data in 0.2–10 keV energy range) and hard X-ray (*Swift*/BAT data in 15–50 keV energy range) of Cen X-3 is shown. Phase zero corresponds to the mid-eclipse time of the pulsar. The PN data is normalized with respect to the *Swift*/BAT data at the out-of-eclipse phase for the comparison of eclipse-egress and out-of-eclipse at soft and hard X-rays.

curves cover a part of eclipse, eclipse-egress and out of eclipse phases of the binary orbit for a total exposure of about 66 ks. The 100 s binned light curve, obtained from PN event data, is shown in Fig. 1. The mid-eclipse time, beginning of eclipse-egress and the end-of-eclipse of the pulsar are shown in the figure. The orbital parameters used to determine the mid-eclipse time and end-of-eclipse time are taken from Paul et al. (2005). The figure shows that the eclipse egress is smooth and instead of a single linear increase in flux, the count rate profile can be described as several piece-wise linear segments from the eclipse to the out of eclipse. Each letter in the figure represents a certain duration for which time-resolved spectral analysis was carried out. The eclipse-egress seen in the PN light curve is unlike the sharp rise in the X-ray flux when the source comes out of eclipse due to the binary companion, as seen in case of SMC X-1 (Raichur & Paul 2010) and LMC X-4 (Naik & Paul 2004). To investigate the peculiar nature of smooth eclipse-egress in Cen X-3 in present analysis, we compare the hard X-ray light curve (in 15–50 keV range) of the pulsar obtained from *Swift*/BAT monitoring data. The entire *Swift*/BAT light curve of Cen X-3 was folded with the orbital period of the pulsar and shown in Fig. 2 along with the normalized PN light curve in 0.2–10 keV energy band. In the figure, phase zero corresponds

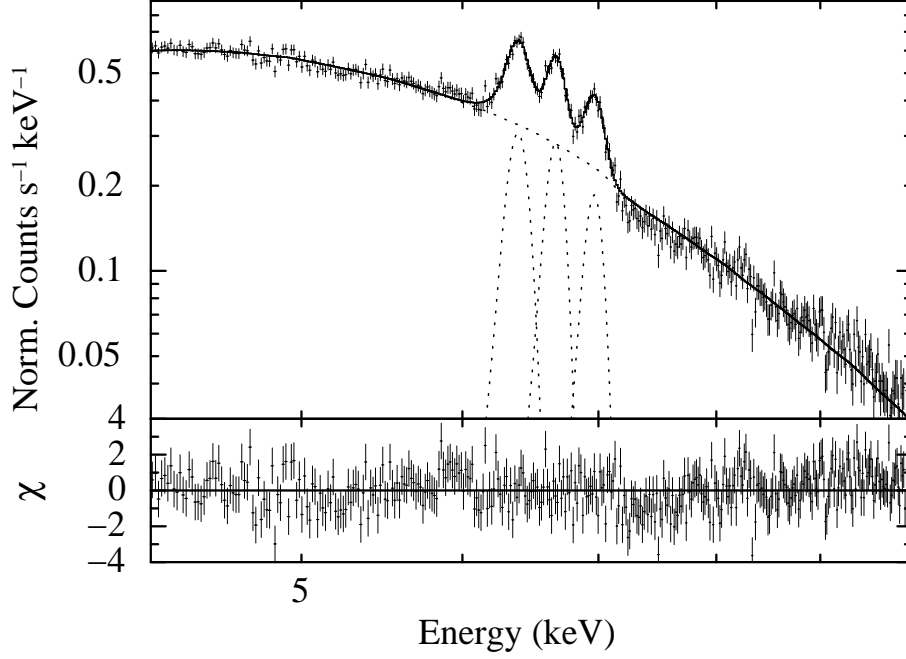


**Figure 3.** Energy spectrum of Cen X-3 obtained with the MOS-2 detector of the *XMM – Newton* observations, along with the best-fitting model comprising a power law continuum component and three narrow iron line emissions. The bottom panel shows the contributions of the residuals to the  $\chi^2$  for each energy bin for the best-fitting model.

to the mid-eclipse time (as shown in Fig. 1). Normalization of the PN light curve was done to compare the orbital modulation such as duration of the eclipse-egress at soft and hard X-rays. One can see that the eclipse-egress is very sharp in hard X-rays in contrast to what observed in soft X-rays. This confirms that the beginning of eclipse-egress and out-of-eclipse phases is different at soft and hard X-rays because of absorption/scattering which is different in different energy bands and intensity states of Cen X-3.

After appropriate background subtraction, simultaneous spectral fitting was performed using the PN and MOS-2 spectra. The PN and MOS-2 spectra for the entire observations were fitted with a power-law continuum model with interstellar absorption and a Gaussian function for the Fe I  $K\alpha$  emission line at 6.4 keV. All the model parameters other than the relative normalization were tied together for both the detectors. The spectral fitting was poor with the presence of positive residuals at low energies representing the emission lines from Ne, Mg, Si, S etc. and at 6.7 keV (Fe XXV  $K\alpha$  line) and 6.97 keV (Fe XXVI  $K\alpha$  line). As our aim was to investigate the evolution of iron emission lines at different binary phases, the subsequent spectral fitting was restricted to 4-10 keV energy range. Two additional Gaussian functions were added to the spectral model for 6.7 keV and 6.97 keV iron emission lines. After a careful investigation of the residuals, we found a mismatch in the value of line energies between MOS-2 and PN spectra of the pulsar.

**Table 1.** Best-fit spectral parameters of Cen X-3 during entire *XMM – Newton* observations. The errors quoted are for  $1\sigma$ .

Parameter	Value
$N_H$ ( $10^{22}$ atoms $\text{cm}^{-2}$ )	$8.7 \pm 0.6$
Power-law photon index	$0.87 \pm 0.03$
Iron line energy (in keV)	$6.4 \pm 0.1$
Iron line width $\sigma_1$ (in keV)	$0.04 \pm 0.01$
6.4 keV line equ. width (in eV)	$156 \pm 4$
6.4 keV line flux <sup>a</sup>	$3.38 \pm 0.12$
Iron line energy (in keV)	$6.67 \pm 0.01$
Iron line width $\sigma_2$ (in keV)	$0.02 \pm 0.01$
6.67 keV line equ. width (in eV)	$129 \pm 3$
6.67 keV line flux <sup>a</sup>	$3.35 \pm 0.11$
Iron line energy (in keV)	$6.97 \pm 0.01$
Iron line width $\sigma_3$ (in keV)	$0.02 \pm 0.01$
6.97 keV line equ. width (in eV)	$124 \pm 5$
6.97 keV line flux <sup>a</sup>	$2.79 \pm 0.11$

<sup>a</sup> : Iron line flux is in the units of  $10^{-12}$  ergs  $\text{cm}^{-2}$   $\text{s}^{-1}$

After communication with the *XMM – Newton* help desk, we found that the problem was known to EPIC calibration team though they had not done any changes at the high energy end of the calibration. Considering this, we tried to fit the MOS-2 and PN spectra separately with above model and found that all three iron emission lines were present in both the cases. However, the line energies obtained from MOS-2 spectrum were found to be close to the corresponding values obtained from atomic database. Therefore, we used MOS-2 data for further spectral analysis. After fitting the MOS-2 spectrum with above model, we found that the spectrum was hard with a photon index of  $\sim 0.8$ . Though the spectral fitting was done in 4-10 keV energy range, an interstellar absorption component was required to fit the spectrum and the value of equivalent hydrogen column density was found to be  $8.7 \times 10^{22}$  atoms  $\text{cm}^{-2}$ . Considering the energy range of spectral fitting (i.e. 4-10 keV) and the wide range of source count rate during the observations presented here, the value of estimated hydrogen column density may not be accurate enough to draw any reliable conclusion. The average spectra, along with the line components are shown in Fig. 3 and the best-fit spectral-fitting parameters obtained are given in Table 1.

To investigate the changes in various spectral parameters, specifically the iron emission lines at different orbital phases of the binary system, we divided the entire light curve into various segments as marked by letters in Fig. 1. The source spectrum for each segment was extracted from PN and MOS-2 event data as described above. The same EPIC response files and background spectrum are used to fit the time resolved spectra for all the segments. A power-law model with

three Gaussian functions was used for the spectral fitting to the data of all segments in 4.0–10.0 keV energy range. The energy spectra for eight segments covering eclipse, eclipse-egress and out-of-eclipse, are shown in Fig. 4. The value of power-law photon index was found to be lower (in the range of 0.6–0.7) during the eclipse segments which increased gradually with increase in source flux and became maximum ( $\sim 1.14$ ) when the source was completely out-of-eclipse. Gradual increase in the power-law normalization was also seen during the entire observations. The presence of three iron emission lines with variable strengths are clearly seen in all the panels. It can be seen that the 6.4 keV iron line is weakest during the eclipse. The other lines are stronger compared to the 6.4 keV line during the eclipse and eclipse-egress. The change in iron line parameters such as line flux and equivalent widths during the entire observations are shown in Fig. 5 along with the source light curve, hard X-ray flux in 5–10 keV energy range, power-law photon index and power-law normalizations. It can be seen from the figure that the flux of all three iron emission lines increases gradually along with the hard X-ray flux though the increase in 6.4 keV flux is larger compared to the 6.7 keV and 6.9 keV lines. However, the change in the line equivalent widths shows different trend for the three emission lines. The equivalent width of the 6.4 keV line increases along with the X-ray flux where as in the case of other two emission lines, it is maximum during the eclipse i.e. minimum hard X-ray flux and is lesser as the neutron star comes out of the eclipse.

In order to evaluate the evolution of the three iron emission lines as the pulsar comes out of the eclipse, we normalized the line flux of 6.7 keV and 6.9 keV lines to that of the 6.4 keV line. The resulting flux ratios are shown in Fig. 6. For a comparison of the relative flux evolution of three iron lines with the source flux, we presented the source light curve (top panel) along with the flux ratios. The second and third panels show the ratios of 6.4 keV line flux to that of the 6.7 keV and 6.9 keV lines, respectively whereas the bottom panel shows the ratio of 6.7 keV flux to that of 6.9 keV line. The ratio of the 6.7 keV line flux and 6.9 keV line flux (bottom panel) was found to be approximately constant over the entire observations. This is a clear evidence that the size of the region in which the 6.7 keV and 6.9 keV lines are produced is comparable to the size of the companion star and not affected significantly due to the eclipse. Significant rise in the flux ratios of 6.4 keV line to that of other two lines (second and third panels) as the pulsar comes out of the eclipse confirms the 6.4 keV line emitting region to be located at the close proximity of the pulsar. Based on these findings, it is certain that the origin of the three emission lines are different. The 6.4 keV line is originated from a region that is close to the pulsar where as the origin of the other two lines is further away from the pulsar, at a distance comparable to the size of the companion star.

### 3. Discussion

The broad-band spectrum of accretion powered X-ray pulsars are generally described by a power-law, broken power-law or power-law with high energy cutoff continuum models. In some cases, the pulsar spectrum has also been described by the NPEX continuum model (Mihara 1995; Makishima et al. 1999; Terada et al. 2006; Naik et al. 2008 and references therein). Recently, it has been found that the spectra of several HMXB pulsars are being described by partially absorbed

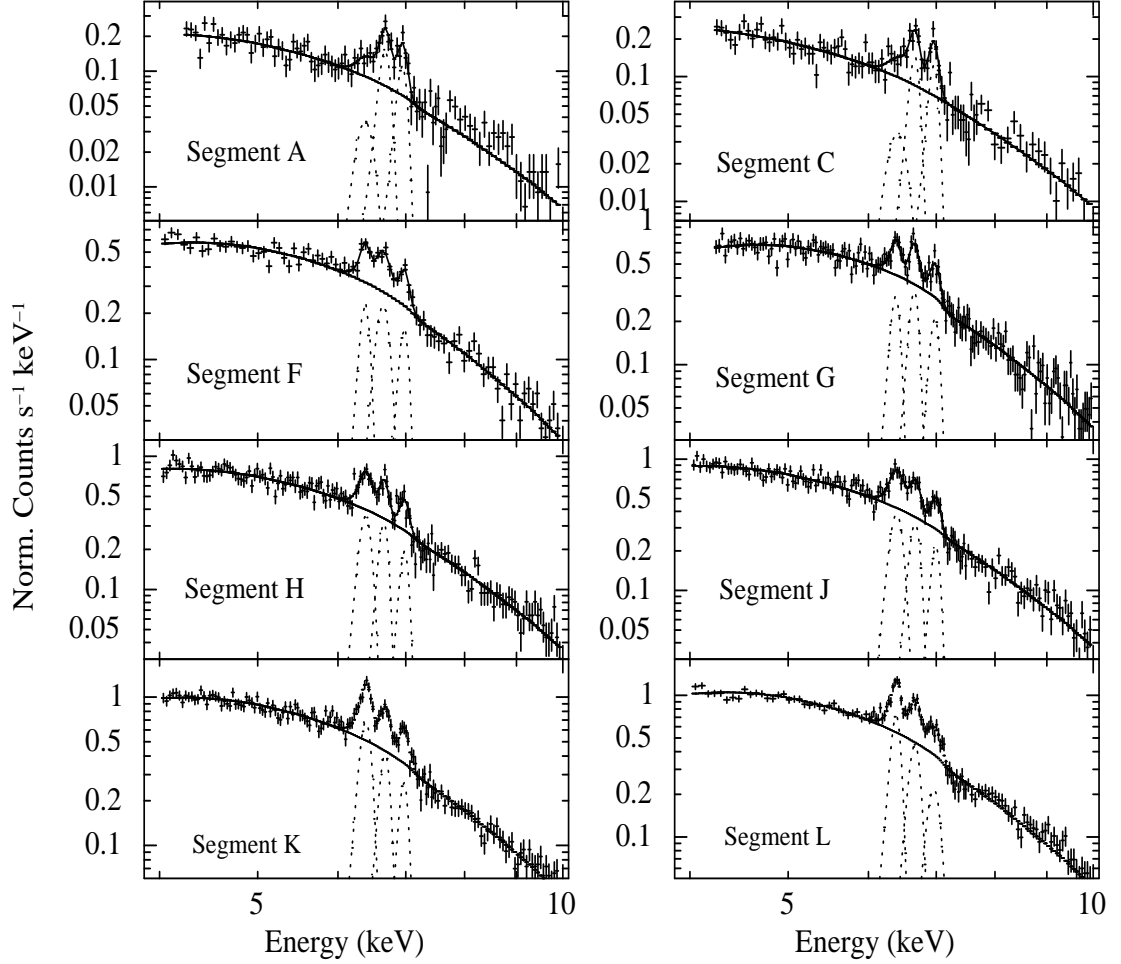


**Figure 4.** Time resolved energy spectra of Cen X-3 obtained with the MOS-2 detector of the *XMM – Newton* observations, along with the best-fit model comprising a power law continuum model, three iron line emissions at 6.4 keV, 6.7 keV, and 6.97 keV. Each spectrum represents different segments of the entire observations (as noted in the figure) from which data were used for spectral fitting. The variation in the continuum level and also the iron emission lines are seen in the spectra.



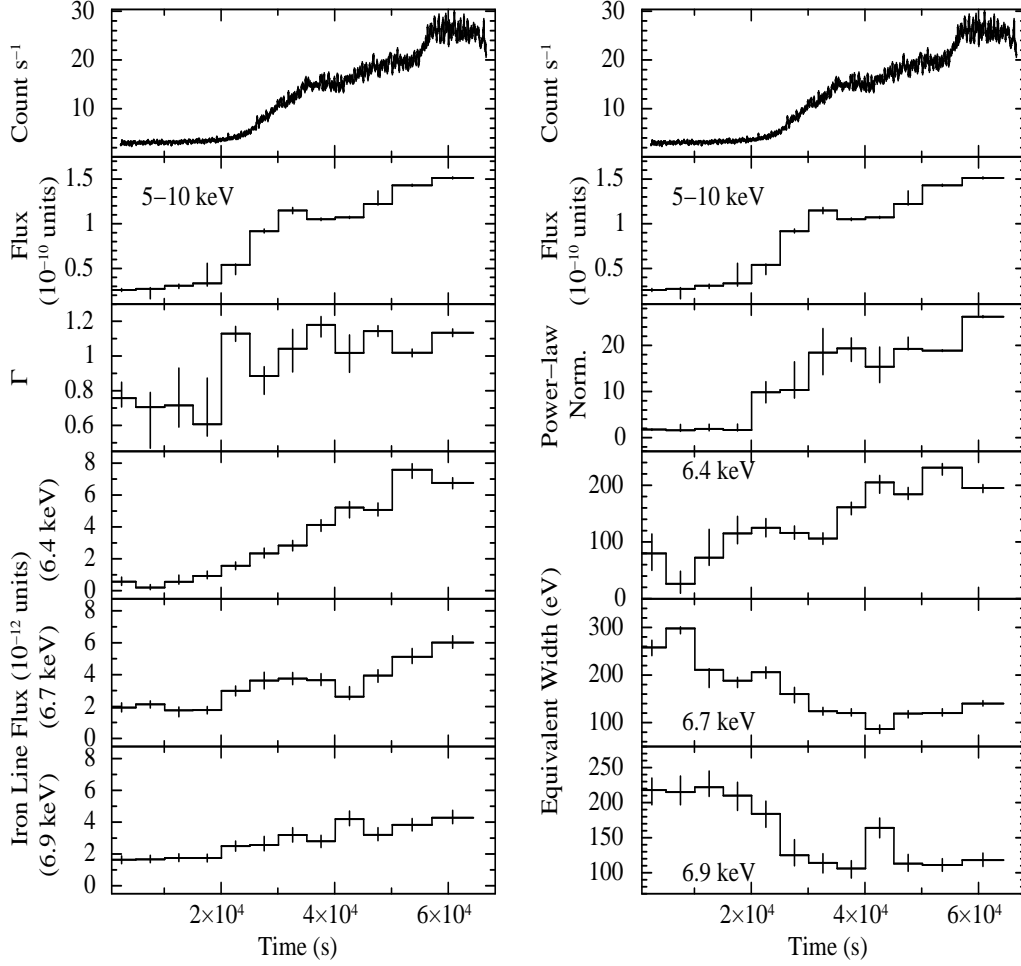


**Figure 5.** Iron emission line parameters obtained from the time resolved spectroscopy of *XMM – Newton* observations of Cen X-3. The errors shown in the figure are estimated for  $1\sigma$  confidence level. The top two panels show source light curve and observed flux in 5–10 keV energy range (in units of  $10^{-10}$  ergs  $\text{cm}^{-2}$   $\text{s}^{-1}$ ), respectively. The change in the values of power-law photon index and normalization with time are shown in third panels (left side and right side), respectively. The bottom three panels in left side show the change in estimated line flux (in  $10^{-12}$  ergs  $\text{cm}^{-2}$   $\text{s}^{-1}$  units) where as the bottom three panels in right side show the variation in the equivalent widths for three iron emission lines during the entire observations.

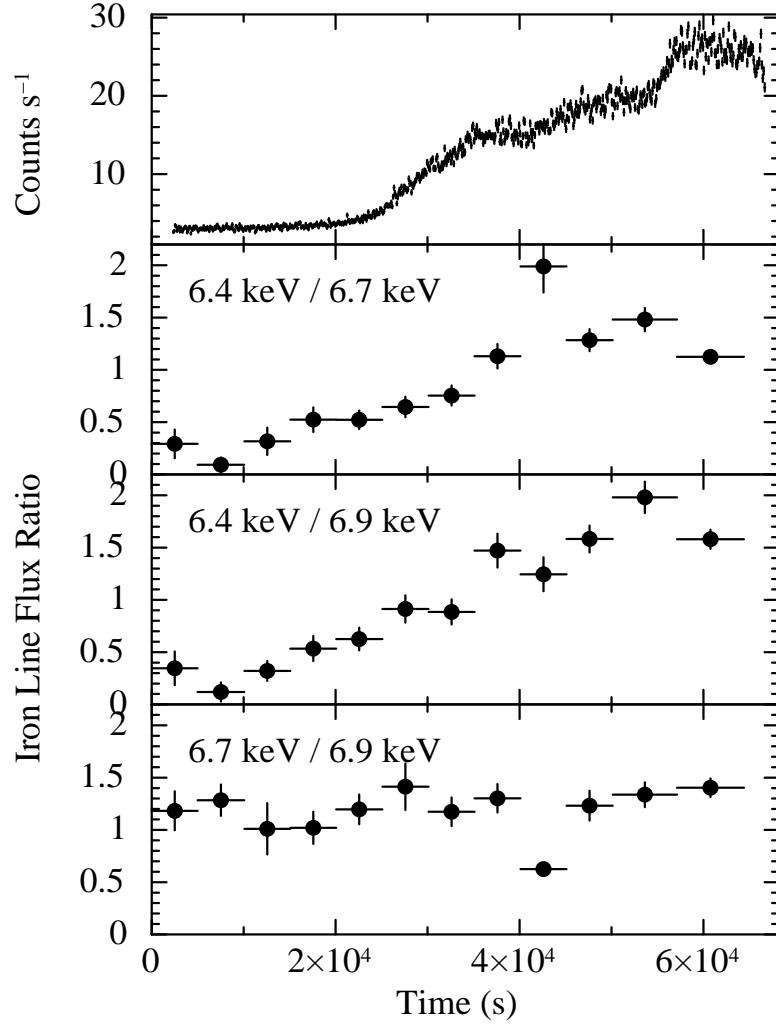


**Figure 6.** Ratios of the flux of 6.4 keV, 6.7 keV and 6.9 keV iron emission lines along with the source light curve during the entire *XMM-Newton* observations. Second and third panels show the ratios of 6.4 keV line flux to that of 6.7 keV and 6.9 keV line whereas the fourth panel shows the flux ratio of 6.7 keV line to 6.9 keV line.

high energy cutoff power-law continuum model (Naik et al. 2011, Devasia et al. 2011, Maitra et al. 2012 and references therein). The partial covering model consists of two power-law continua with a common photon index but with different absorbing hydrogen column densities. The choice of the appropriate continuum model, therefore, is very important to understand the properties of the pulsars. A detailed broad band spectral analysis of the HMXB Cen X-3 with the *Suzaku* observatory covering nearly one orbital period showed that the pulsar spectrum was well described by a partial covering power-law model with high energy cut-off and three Gaussian functions for iron emission lines (Naik, Paul & Ali 2011). As the range of spectral fitting presented here in this paper is limited from 4 to 10 keV to investigate the evolution of iron emission lines, a single power-law continuum model is used in the analysis.

The 6.4 keV  $K\alpha$  iron emission line has been observed in the spectrum of many X-ray binary pulsars. In some of the binary pulsars, emission lines at 6.7 keV (e.g. Cen X-3; Ebisawa et al. 1996), 6.95 keV (e.g. GX 1+4; Paul et al. 2005), 7.1 keV (e.g. GX 1+4; Naik, Paul & Callanan 2005) are also seen. It is known that the X-ray spectrum of Cen X-3 is complex in 6.0-7.5 keV range because of the presence of several iron emission lines with variable strengths at different orbital phases. As in case of many other pulsars, the iron  $K\alpha$  emission line at  $\sim 6.4$  keV is always present in the spectra of Cen X-3. Along with this line, there are several structures around  $\sim 6.6$  keV, 6.9 keV, 7.1 keV etc. Ebisawa et al. (1996), Naik, Paul & Ali (2011) detected the presence of 6.67 keV and 6.95 keV lines in Cen X-3 with *ASCA* and *Suzaku* data, respectively. Iaria et al. (2005) also detected the Fe XXV He-like triplet with the grating data from Chandra. All three iron emission lines (as described above) are clearly detected at all segments of the *XMM – Newton* observations used in this paper. Tugay & Vasylenko (2009) used the same observations that are used in the present study, to estimate the neutron star parameters such as mass of the compact object, the inclination of the accretion disc, inner and outer radii of the disc by applying the geometric model of the relativistic accretion disc to the iron emission lines. The authors tried to study the spectral variability of the pulsar by dividing the entire observations to two segments (eclipse and eclipse-egress) and compared the results with that obtained from the *ASCA* observations. In the process, the intensity variations of the three iron emission lines were detected, the largest variation was for the 6.4 keV  $K\alpha$  emission line. The *ASCA* observations of the pulsar covered the pre-eclipse, eclipse-ingress, eclipse, and eclipse-egress using which the line parameters were derived to study the origin of the lines (Ebisawa et al. 1996). In this paper, however, a systematic and detailed investigation of the evolution of three iron emission lines was carried out using the same *XMM – Newton* observations as was used by Tugay & Vasylenko (2009). In the process, as many as twelve measurements of line parameters were made during the eclipse, eclipse-egress and out-of-eclipse phase of the binary orbit of the pulsar.

In the present work, we found that the intensity of the 6.4 keV iron emission line varies significantly with the 5-10 keV source flux. During the eclipse, it was minimum ( $\sim 2 \times 10^{-13}$  ergs cm $^{-2}$  s $^{-1}$ ) which increased to maximum ( $\sim 8 \times 10^{-12}$  ergs cm $^{-2}$  s $^{-1}$ ) during the out-of-eclipse phase. The flux of other two lines at 6.7 keV and 6.9 keV, however, did not increase at the same rate as compared to that of 6.4 keV line. The 6.7 keV and 6.9 keV line flux increased by a factor of  $\sim 3$  compared to an increase in 6.4 keV line flux by a factor of  $\sim 40$ . The 6.7 keV line flux was increased from  $\sim 2 \times 10^{-12}$  ergs cm $^{-2}$  s $^{-1}$  (during eclipse) to  $\sim 6 \times 10^{-12}$  ergs cm $^{-2}$  s $^{-1}$  (during the

out-of-eclipse phase). The increase in the 6.9 keV line flux was similar to that of the 6.7 keV flux. The change in flux of iron emission line flux for all three lines are gradual as the 5-10 keV source flux from the eclipse to out-of-eclipse phase of the orbital period. The equivalent widths of 6.7 and 6.9 keV lines were maximum during the eclipse which became minimum during the out-of-eclipse phase, whereas it is opposite in case of the 6.4 keV line. The relative flux variabilities of the three iron emission lines are clearly shown in Fig. 6. Significant increase in the 6.4 keV line flux compared to that of 6.7 keV and 6.9 keV lines as the pulsar moves from the eclipse to out-of-eclipse phase confirms that the 6.4 keV line emitting region is being obscured during the eclipse. As the pulsar comes out of the eclipse, the  $K\alpha$  line emitting region gradually becomes visible and enhances the flux of the emission line. However, the marginal increase in the flux of other two emission lines as the pulsar moves out of eclipse suggest that the corresponding line emitting regions are spread over large area and distributed far away from the pulsar. This allows a small fraction of the 6.7 keV and 6.9 keV energy photons to be blocked by the eclipse due to the companion star. The results confirm that the origin of the 6.4 keV emission line is different from that of the 6.7 and 6.9 keV emission lines in Cen X-3. The 6.4 keV line is originated due to the fluorescence of cold and dense material that is very close to the neutron star where as the other two lines are produced in a region that is far from the neutron star, probably in the highly photo-ionized wind of the companion star or in the accretion disk corona.

### Acknowledgments

The research work at Physical Research Laboratory is funded by the Department of Space, Government of India. This research has made use of data obtained through the High Energy Astrophysics Science Archive Research Center Online Service, provided by the NASA/Goddard Space Flight Center. The authors thank both the anonymous reviewers for their useful suggestions and comments which helped to improve the paper.

### References

- Audley M. D., et al., 1996, *ApJ*, 457, 397  
 Boella G., Butler R., C., Perola G., Piro L., Scarsi L., Bleeker J. A. M., 1997, *A&AS*, 122, 299  
 Burderi L., Di Salvo T., Robba N. R., La Barbera A., Guainazzi M., 2000, *ApJ*, 530, 429  
 Chodil G., Mark H., Rodrigues R., Seward F., Swift C.D., Hiltner W.A., Wallerstein G., Mannery E.J., *Phys. Rev. Lett.*, 19, 681  
 Choi C. S., Nagase F., Makino F., Dotani T., Kitamoto S., Takahama S., 1994, *ApJ*, 437, 449  
 Day C. S. R., Stevens I. R., 1993, *ApJ*, 403, 322  
 Devasia J., James M., Paul B., Indulekha K., 2011, *MNRAS*, 417, 348  
 Ebisawa K., Day C. S. R., Kallman T. R., Nagase F., Kotani T., Kawashima K., Kitamoto S., Woo J. W., 1996, *PASJ*, 48, 425  
 Giacconi R., Gursky H., Kellogg E., Schreier E., Tananbaum H., 1971, *ApJ*, 167, L67  
 Heindl W. A., Gruber D. E., Rothschild R. E., Crannell C. J., Lang F. L., Kaplan L., 1999, *BAAS*, 31, 715  
 Hutchings J. B., Cowley A. P., Crampton D., van Paradijs J., White N. E., 1979, *ApJ*, 229, 1079  
 Iaria R., Di Salvo T., Robba N. R., Burderi L., Lavagetto G., Riggio A., 2005, *ApJ*, 634, L161  
 Inam S. C., Baykal A., 2005, *MNRAS*, 361, 1393

- Iping R. C., Petterson J. A., 1990, *A&A*, 239, 221
- Jansen F., et al., 2001, *A&A*, 365, L1
- Jimenez-Garate M. A., Hailey C. J., den Herder J. W., Zane S., Ramsay G., 2002, *ApJ*, 578, 391
- Kelley R. L., Rappaport S., Clark G. W., Petro L. D., 1983, *ApJ*, 268, 790
- Krzeminski W., 1974, *ApJ*, 192L, 135
- Leahy D. A., 2001, *ApJ*, 547, 449
- Maitra C., Paul B., Naik S., 2012, *MNRAS*, 420, 2307
- Makishima K., Mihara T., Nagase F., Tanaka, Y., 1999, *ApJ*, 525, 978
- Mihara T., 1995, Ph.D. Thesis, University of Tokyo
- Mukherjee U., Paul B., 2004, *A&A*, 427, 567
- Nagase F., 1989, *PASJ*, 41, 1
- Nagase F., Corbet R. H. D., Day C. S. R., Inoue H., Takeshima T., Yoshida K., Mihara T., 1992, *ApJ*, 396, 147
- Naik S. Paul B., 2003, *A&A*, 401, 265
- Naik S. Paul B., 2004, *ApJ*, 600, 351
- Naik S., Paul B., Callanan P. J., 2005, *ApJ*, 618, 866
- Naik S., et al., 2008, *ApJ*, 672, 516
- Naik S., Paul B., Kachhara C., Vadawale S. V., 2011, *MNRAS*, 413, 241
- Naik S., Paul B., Ali Z., 2011, *ApJ*, 737, 79
- Ogilvie G. I., Dubus G., 2001, *MNRAS*, 320, 485
- Orlandini M., 2006, *AdSpR*, 38, 2742
- Paul B., Nagase F., Endo T., Dotani T., Yokogawa J., Nishiuchi M., 2002, *ApJ*, 579, 411
- Paul B., Raichur H., Mukherjee U., 2005, *A&A*, 442, L15
- Paul B., Dotani T., Nagase F., Mukherjee U., Naik S., 2005, *ApJ*, 627, 915
- Raichur H., Paul B., 2010, *MNRAS*, 401, 1532
- Santangelo A., del Sordo S., Segreto A., dal Fiume D., Orlandini M., Piraino S., 1998, *A&A*, 340, L55
- Schreier E., Levinson R., Gursky H., Kellogg E., Tananbaum H., Giacconi R., 1972, *ApJ*, 172, L79
- Scott D., Leahy D. 1999, *ApJ*, 510, 974
- Shafer R. A., Haberl F., Arnaud K. A., 1989, *XSPEC: An X-ray Spectral Fitting Package*, ESA TM-09, ESA, Paris
- Takeshima T., Dotani T., Mitsuda K., Nagase F., 1991, *PASJ*, 43L, 43
- Tanaka Y., Inoue H., Holt S. S., 1994, *PASJ*, 46, L37
- Terada Y., et al., 2006, *ApJ*, 648, L139
- Tjemkes S. A., van Paradijs J., Zuiderwijk E. J., 1986, *A&A*, 154, 77
- Tugay A. V., Vasylenko A. A., 2009, in Choliy V. Ya., Ivashchenko G., eds, *YSC'16 Proceedings of Contributed Papers*, p. 58
- Vrtilek S. D., Raymond J. C., Boroson B., Kallman T., Quaintrell H., McCray R., 2001, *ApJ*, 563, L139
- Weisskopf M. C., Brinkman B., Canizares C., Garmire G., Murray S., Van Speybroeck L. P., 2002, *PASP*, 114, 1
- White N. E., Swank J. H., Holt S. S., 1983, *ApJ*, 270, 711
- White N. E., Nagase F., Parmar A. N. 1995, in Lewin W. H. G., van Paradijs J., van den Heuvel E.P.J. eds, *X-Ray Binaries*, Cambridge University Press, Cambridge, p. 1
- Wojdowski P. S., Liedahl D. A., Sako M., Kahn S. M., Paerels F., 2003, *ApJ*, 582, 959